Cell Reports
Methods

Report

In situ microwave fixation provides an instantaneous snapshot of the brain metabolome

Graphical abstract

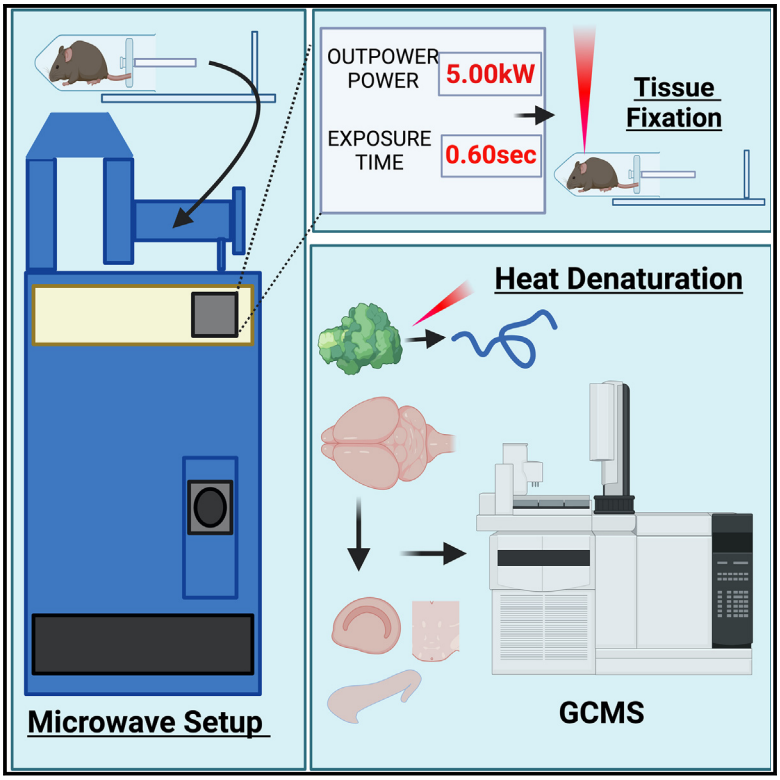

Authors

Jelena A. Juras, Madison B. Webb, Lyndsay E.A. Young, ..., Matthew S. Gentry, Bret N. Smith, Ramon C. Sun

Correspondence

ramonsun@ufl.edu

In brief

Juras et al. demonstrate the use of a high-power, focused microwave for the simultaneous euthanasia and fixation of mouse brain to preserve metabolite pools prior to surgical dissection and metabolomic studies. They apply this approach to characterize brain glucose metabolism in a mouse model of type 1 diabetes mellitus.

Highlights

- Direct *in situ* fixation of rodent brain by high-powered, focused microwave
- Microwave fixation preserves glycogen and glycolytic metabolites
- Glucose hypometabolism demonstrated type 1 diabetes mellitus mouse model brains
- Decreased enzyme levels observed in the same T1DM mouse model

Juras et al., 2023, Cell Reports Methods *3*, 100455
April 24, 2023
https://doi.org/10.1016/j.crmeth.2023.100455

CellPress

Cell Reports Methods

CellPress
OPEN ACCESS

Report

In situ microwave fixation provides an instantaneous snapshot of the brain metabolome

Jelena A. Juras,[1] Madison B. Webb,[2] Lyndsay E.A. Young,[2,3] Kia H. Markussen,[2] Tara R. Hawkinson,[1,4] Michael D. Buoncristiani,[1] Kayli E. Bolton,[2] Peyton T. Coburn,[2] Meredith I. Williams,[2] Lisa P.Y. Sun,[1,3] William C. Sanders,[2] Ronald C. Bruntz,[2] Lindsey R. Conroy,[1,3] Chi Wang,[3,5] Matthew S. Gentry,[2,3,4,7] Bret N. Smith,[1,6] and Ramon C. Sun[1,3,4,7,8,*]

[1]Department of Neuroscience, University of Kentucky, College of Medicine, Lexington, KY 40536, USA
[2]Department of Molecular and Cellular Biochemistry, University of Kentucky, College of Medicine, Lexington, KY 40536, USA
[3]Markey Cancer Center, University of Kentucky, Lexington, KY 40536, USA
[4]Department of Biochemistry and Molecular Biology, University of Florida, College of Medicine, Gainesville, FL 32611, USA
[5]Division of Biostatics, Department of Internal Medicine, University of Kentucky, College of Medicine, Lexington, KY 40536, USA
[6]Department of Biomedical Sciences, Colorado State University, Fort Collins, CO 80523, USA
[7]Center for Advanced Spatial Biomolecule Research, University of Florida, College of Medicine, Gainesville, FL 32611, USA
[8]Lead contact
*Correspondence: ramonsun@ufl.edu
https://doi.org/10.1016/j.crmeth.2023.100455

MOTIVATION Brain metabolism directly connects to brain physiology and neuronal function, but challenges remain to capturing an accurate snapshot of the physiological brain metabolome in healthy and diseased rodent models. One challenge is that brain metabolism does not cease at the moment of animal sacrifice, and in conventional protocols, there is typically a delay between animal sacrifice and surgical isolation of the tissue for snap freezing and/or fixation, during which time postmortem conditions such as hypoxia may start to influence the pools of metabolites in the sample. To overcome this barrier, we employed high-power, focused microwave for the simultaneous euthanasia and fixation of mouse brain tissue *in situ* to preserve metabolite pools prior to surgical removal and dissection of brain regions.

SUMMARY

Brain glucose metabolism is highly heterogeneous among brain regions and continues postmortem. In particular, we demonstrate exhaustion of glycogen and glucose and an increase in lactate production during conventional rapid brain resection and preservation by liquid nitrogen. In contrast, we show that these postmortem changes are not observed with simultaneous animal sacrifice and *in situ* fixation with focused, high-power microwave. We further employ microwave fixation to define brain glucose metabolism in the mouse model of streptozotocin-induced type 1 diabetes. Using both total pool and isotope tracing analyses, we identified global glucose hypometabolism in multiple brain regions, evidenced by reduced ^{13}C enrichment into glycogen, glycolysis, and the tricarboxylic acid (TCA) cycle. Reduced glucose metabolism correlated with a marked decrease in GLUT2 expression and several metabolic enzymes in unique brain regions. In conclusion, our study supports the incorporation of microwave fixation for more accurate studies of brain metabolism in rodent models.

INTRODUCTION

Brain metabolism is the biochemical basis of memory, cognition, and central nervous system (CNS)/peripheral neuronal signaling. The brain consumes approximately 20% of circulating glucose[1] and although debated, neurons are proposed to be the major glucose-consuming cells of the brain.[2,3] Glucose metabolism of the brain can be subdivided into catabolic or anabolic processes. Catabolic processes involve the breakdown of glucose for energy production via glycolysis and the tricarboxylic acid (TCA) cycle.[4] Neurotransmitters such as GABA, glutamate, and aspartate can be *de novo* synthesized through glucose catabolism.[5] In contrast, anabolic glucose metabolism utilizes either glucose or glucose derivatives for the synthesis of lipids,[6]

complex carbohydrates such as glycans,[7] chondroitin,[8] and heparan sulfate biopolymers,[9] all of which are critical biomass and structural components of the brain. Given that brain glucose participates in a myriad of metabolic processes from bioenergetics to neurotransmitter and biomass production, it is difficult to decipher which downstream processes are perturbed from reduced 2-deoxyglucose uptake and are unique to disease pathogenesis.

Glucose hypometabolism is characterized by reduced uptake of 2-fluorodeoxyglucose (FDG), imaged by positron emission tomography (PET), and is a common pathological feature shared among multiple neurological disorders such as Alzheimer's disease (AD),[10] Parkinson's disease,[11] temporal lobe epilepsy,[12] inherited pediatric neurodegenerative diseases,[13] and peripheral diseases such as type 1 diabetes.[14] Recently, the glycolysis-lactate axis has been highlighted as a key pathway perturbed in disease-associated microglia during AD progression.[15,16] Further, we found that protein hyperglycosylation, an anabolic product of glucose metabolism, is a hallmark of AD in both human and mouse specimens.[17] Collectively, these studies highlight the potential of alternative metabolic fates of glucose in neurodegenerative diseases. Conversely, orphan neurological disorders such as Glut1 deficiency,[13] PDH deficiency,[18] and Lafora disease all present with reduced glucose uptake on FDG-PET,[19] reduced oxidative phosphorylation, and protein glycosylation, and patients are prone to epileptic seizures and accelerated neurodegeneration.[18,20] Therefore, clinical diagnosis of glucose hypometabolism and the downstream glucose metabolic alterations differ based on underlying disease pathology, highlighting the importance of accurately capturing physiological metabolite phenotypes in human and experimental models.

Currently, many techniques to accurately capture physiological brain metabolism in rodents *in vivo* rely on nuclear magnetic resonance (NMR),[21–23] wherein mice are anesthetized, and live animals are used to study metabolic parameters. Metabolite coverage captured by *in vivo* NMR is limited due to technical limitations.[24,25] Thus, large-scale metabolomics studies of the brain require rapid dissection of brain regions postmortem followed by cryo-preservation and mass spectrometry detection of metabolites.[20,26,27] Postmortem surgical removal of the brain ranges from 90 s to several minutes depending on the individual performing the resection. It is well documented that metabolism changes postmortem,[28,29] and the rates of metabolic flux through glycolysis and the TCA cycle occur in seconds.[30–32] Furthermore, artificial tissue hypoxia has been reported in mice following cervical dislocation,[33] decapitation,[34] and CO_2 euthanasia.[35] Brain tissue collection through conventional routes results in glycogen degradation and changes in global protein phosphorylation status.[36,37] A deeper understanding of neuronal function hinges on expanded metabolic pathway coverage, creating a critical need to establish an accurate baseline brain metabolome that excludes residual non-physiological metabolism that occurs during postmortem brain resection.

Microwave fixation of mammalian tissues utilizes water molecule vibration to produce heat,[38] resulting in heat-inactivated protein denaturation and, in principle, stopping all metabolic processes.[39] Indeed, microwave fixation is frequently used in pathology laboratories to preserve mammalian tissues for histopathological analyses.[40] For direct *in situ* tissue fixation of whole animals, a focused microwave has been developed for the rapid inactivation of brain proteins (<0.6 s) and preserves global protein phosphorylation through enzyme inactivation.[37] Since then, this technique has been adapted to study neurotransmitters using *in vivo* NMR in rats.[41–43] In this study, we hypothesized that enzymatic inactivation through microwave fixation would preserve the brain metabolome as well. Herein, we compared *in situ* microwave fixation (0.6 s) with rapid dissection and cryo-preservation of wild-type C57/B6 brain tissues where enzyme inactivation takes about 90+ s. Further, we interrogated the impact of type 1 diabetes mellitus (T1DM) on brain metabolism using the streptozotocin (STZ)-induced hyperglycemia mouse model, compared with vehicle treated,[44,45] and observed profound glucose hypometabolism in the brain of T1DM animals using a focused microwave.

RESULTS

In situ microwave fixation to define brain metabolism

Cellular metabolism continues postmortem in rodents with signs of hypoxia-driven metabolic reprogramming.[29] These metabolic changes are especially true for the brain, and capturing an accurate snapshot of the brain metabolome remains a critical challenge in the field. To test the application of a focused microwave, we designed a two-arm study where euthanasia occurs through either (1) direct decapitation or (2) a focused microwave (Figure 1). In both arms, we performed rapid dissection of the brain followed by cryo-preservation in liquid nitrogen. The major difference between the two arms is that the tissue-fixation or enzyme-inactivation step occurs either during cryo-preservation (CP) for decapitation (~90 s) or focused microwave (FM, ~0.6 s). Peripheral tissues were also collected as controls since they were not subject to microwave radiation. Brain and other tissues from both cohorts of animals were pulverized while in liquid nitrogen by a cryo-mill and prepped for pooled metabolomics analysis by gas chromatography-mass spectrometry (GCMS) for both polar metabolites and biomass.[46–48] For this study, we focused on the cortex (CTX), the hippocampus (HIPP), and the hindbrain dorsal vagal complex (DVC), which contains glucose-sensing neurons that undergo functional neuroplasticity after prolonged hyperglycemia.[49] GCMS metabolomics analyses between the two arms (hereby designated as FM or CP) displayed clear separation by partial least squares-discriminant analysis (PLS-DA) (Figure 1B), and metabolic pathway enrichment analysis suggests changes in glycolysis, gluconeogenesis, TCA cycle, and amino acid metabolism that are shared between FM and CP among all three brain regions (Figure 1C). Targeted metabolite analysis of the central carbon pathway revealed a drastic decrease in glycogen, glucose, and citrate and a profound increase in lactate, malate, and fumarate in the CP arm (Figure 1D). Since the microwave beam of the FM does not have peripheral organs in its path, we included GCMS analyses of the lung, liver, and muscle as controls. We did not observe major changes between FM vs. CP methods in the peripheral organs, with the exception of glucose and glucose-6-phosphate in liver and muscle (Figure S1). Further, FM shows decreased variance within

CellPress
OPEN ACCESS

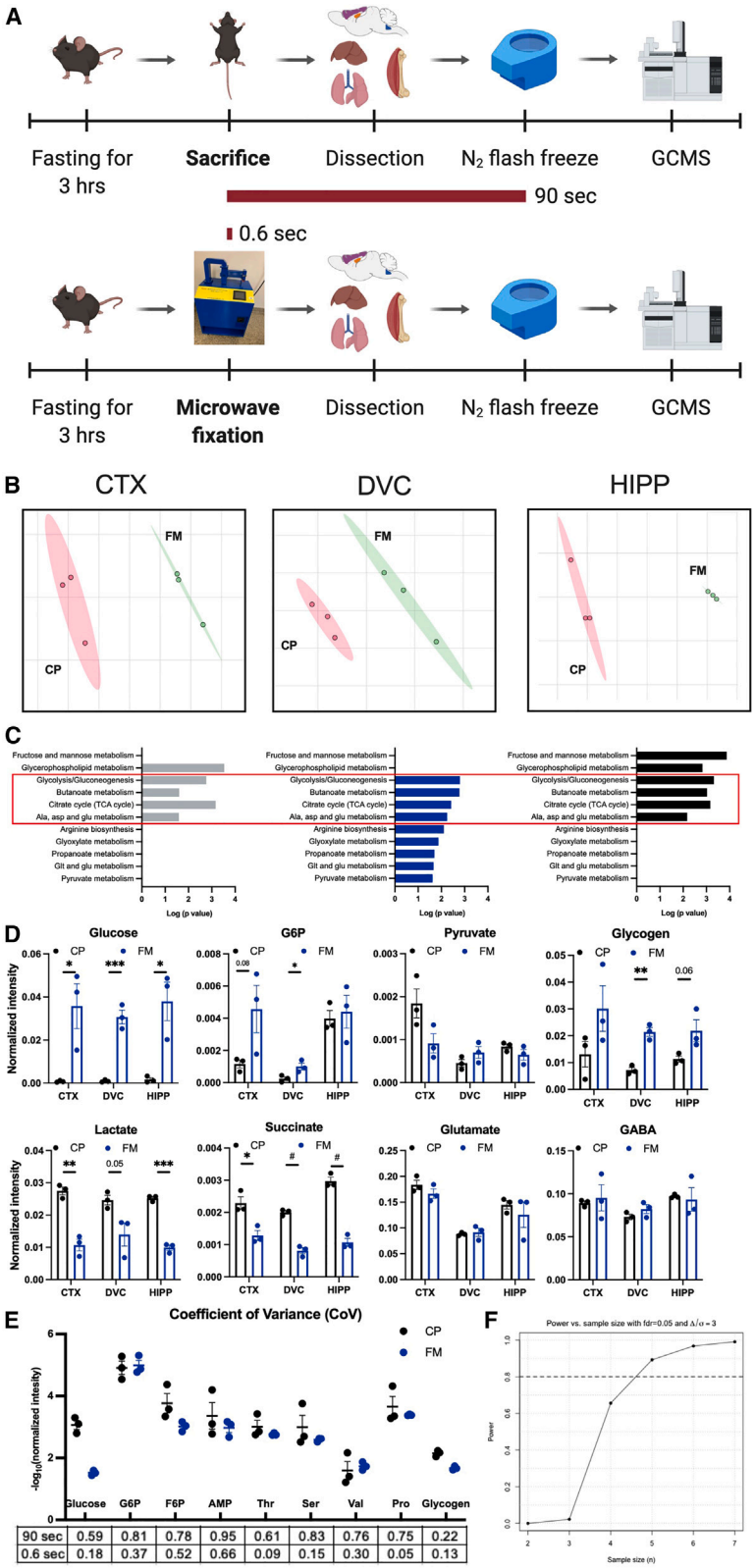

Figure 1. *In situ* FM fixation to study the brain metabolome

(A) Schematic of the experimental design. 6-week-old mice fasted for 3 h and were euthanized by decapitation (top) or microwave fixation (bottom), and brain regions were then dissected, flash frozen, and analyzed by GCMS.

(B) Partial least squares-discriminant analysis (PLS-DA) of cortex (CTX), dorsal vagal complex (DVC), and hippocampus (HIPP) metabolites showing distinct separation between CP and focused microwave (FM).

(C) Pathway analysis comparing CP and FM (performed by Metaboanalyst) of CTX, DVC, and HIPP.

(D) Representative metabolite levels from glycogen metabolism, glycolysis, and TCA cycle between CP and FM. Values are presented as mean ± SEM (n = 3 biological replicates), *p < 0.05, **p < 0.01, ***p < 0.001, #p < 0.0001, analyzed by Student's t test.

(E) Coefficient of variance (CoV) analysis of representative metabolites in (B).

(F) Power analysis indicating the necessary sample size to detect 89% power at 0.05 false discovery rate.

G6P, glucose 6-phosphate; F6P, fructose 6-phospahte; AMP, adenosine phosphate; Thr, threonine; Ser, serine; Val, valine; Pro, proline.

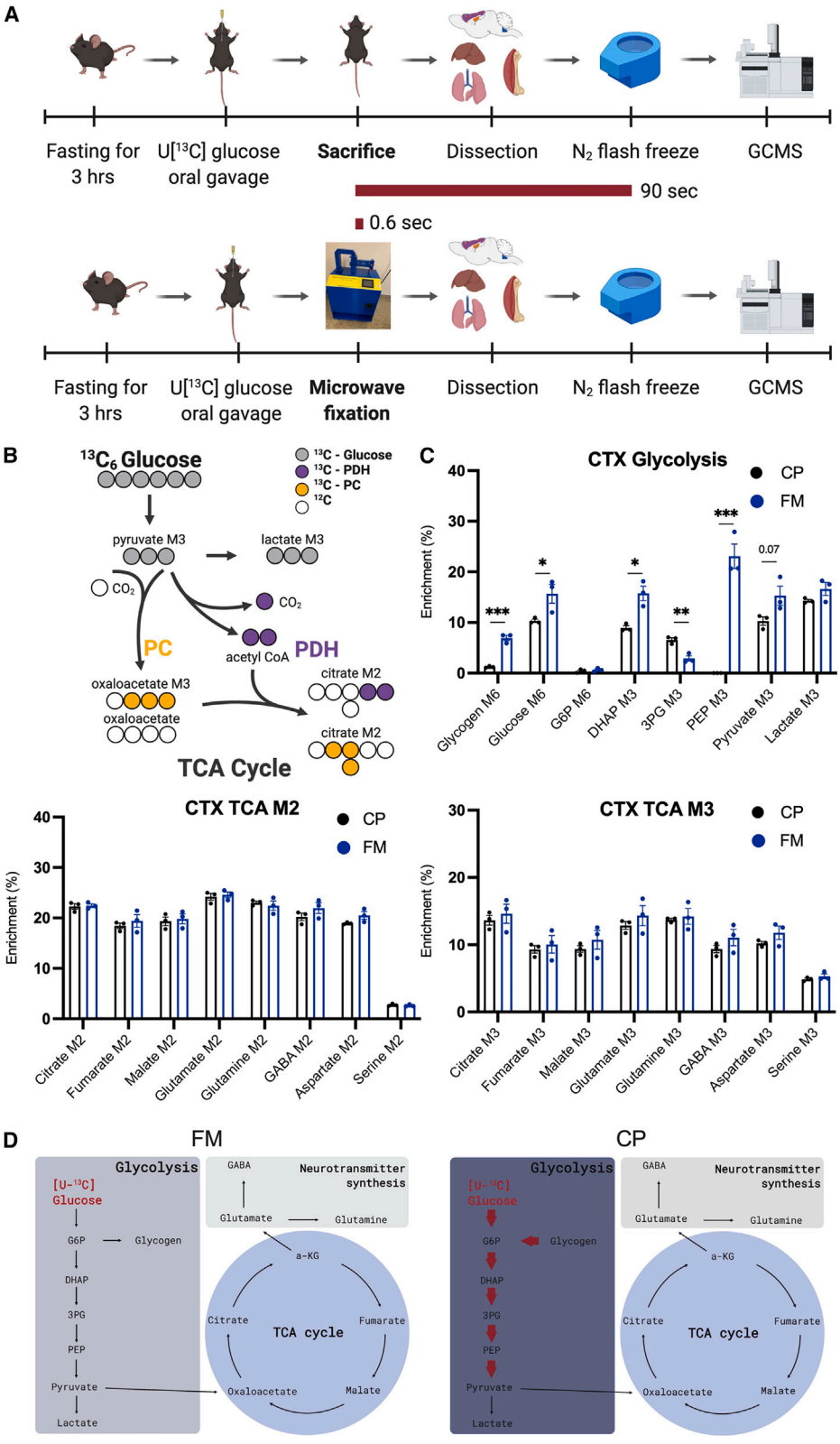

(legend on next page)

groups showing reduced coefficient of variance (CoV) among multiple metabolites (Figure 1E). Finally, based on the current FM dataset (CTX), n = 5/group would provide 89% power to detect those differences with a 5% false discovery rate based on two-sample t tests (Figure 1F).

In situ microwave fixation is compatible with stable isotope tracing

Stable isotopic tracing is invaluable at delineating substrate metabolism and interrogating enzymatic activities.[50,51] To test whether FM fixation is compatible with stable isotope tracing, we performed oral gavage delivery of ^{13}C-glucose using a method previously described[47] and performed euthanasia with either CP (90 s) or FM (0.6 s) in parallel to interrogate isotopic enrichment of central carbon metabolites between the two different brain fixative strategies (n = 3) (Figure 2A). We identified significantly increased enrichment of ^{13}C in glycogen and glycolytic metabolites, including glucose, DHAP, and PEP in the CTX following FM (Figures 2B–2D); however, lactate, citrate, fumarate, malate, and amino acids such as glutamate, glutamine, serine, and GABA remain unchanged between FM and CP (Figure 2C). It is likely that even though total pooled metabolites were changed during CP, both ^{13}C-enriched and ^{12}C-TCA cycle and amino acid metabolites were either consumed or synthesized at the same rate during the 90 s fixation interval. Similarly, we did not observe major changes in ^{13}C-enrichment between FM vs. CP in the lung, liver, and skeletal muscle (Figure S2).

Mouse model of T1DM affects the brain metabolome

T1DM is a peripheral disease that is characterized by the lack of insulin production and persistent high circulating blood glucose. T1DM negatively impacts neurological outcomes, including Alzheimer's-related dementia.[52,53] To define the impact of T1DM on brain glucose metabolism using FM, we utilized the STZ model of insulin impairment and hyperglycemia in mice and performed untargeted analysis of metabolite pools using GCMS. Mice were randomly assigned to two groups (n = 8): one that was injected intraperitoneally (i.p.) with vehicle (citric acid) and another with a single dose of STZ to induce hyperglycemia for 14 days to mimic T1DM (Figures 3A and 3B). Both cohorts of mice were euthanized and fixed by FM followed by surgical resection of multiple brain regions (DVC, pre-blood-brain barrier, and HIPP/CTX post-blood-brain barrier) as well as peripheral organs (muscle and liver). To our surprise, we observed increases only in glucose, glycogen, glucose 6-phosphate, and leucine in different brain regions (Figures 3C and 3D). The majority of the metabolite pools were relatively unchanged in the brain (Figures 3C and 3D). These limited changes were not the case in peripheral organs, as we observed changes in multiple glycolytic and TCA cycle metabolites in the liver (Figure S3); however, it is worth noting that peripheral organs were not in the path of the FM.

Tracing ^{13}C-glucose metabolism in the brain of a T1DM mouse model

Pooled metabolomics analysis does not fully illuminate unique substrate metabolism. T1DM is primarily a disease of hyperglycemia; therefore, it is crucial to define the glucose contribution to different metabolite pools. To assess whether there are differences in glucose metabolism between vehicle- and STZ-treated mice, we performed an additional animal experiment with vehicle- and STZ-treated arms and performed stable isotope tracing of $^{13}C_6$-glucose delivered through oral gavage with collection at either 30 min or 2 h post-gavage (n = 8) (Figures 4A and 4B). All cohorts of mice were fixed *in situ* with FM followed by brain regional dissection and peripheral organ extraction. We observed major decreases in glucose enrichment in central carbon metabolites and *de-novo*-synthesized amino acids. This phenotype is consistent across the CTX, HIPP, and the DVC for both time points (Figures 4C–4E and S4) as well as in peripheral organs (Figure S5). Further, M2 and M3 isotopologes of citrate, malate, fumarate, glutamine, glutamate, and aspartate all exhibited a decrease in the STZ arm compared with the vehicle arm at both time points (Figures 4C–4E and S4). This result suggests down-regulation of pyruvate dehydrogenase and pyruvate carboxylase activity in STZ-induced hyperglycemia in multiple brain regions. Further, when comparing the CTX with the DVC, we observed decreased lactate M3 isotopologue enrichment and increased M2 isotopologue of citrate, malate, and fumarate in the STZ arm (Figures 4F and 4G).

Down-regulation of GLUT2, PDH, and PC proteins in unique neuronal cell layers

The power of stable isotopic tracing is the direct assessment of metabolic enzyme activities through fractional enrichment, i.e., M2 and M3 isotopologues of citrate represent PDH and pyruvate carboxylase (PC) activities, respectively. Mice with STZ-induced hyperglycemia have reduction in M2 and M3 isotopologues of citrate (Figure 4C); therefore, we continued to evaluate glucose transporters and PDH and PC protein expression in cortical and HIPP regions using immunofluorescence (IF) (n = 4). First, we performed IF for GLUT1, GLUT2, and GLUT3 glucose transporters, which have been shown to be affected by hyperglycemia in peripheral tissues.[54–57] We did not observe significant changes in the percentage of positive areas in GLUT1 and

Figure 2. *In situ* FM fixation is compatible with stable isotope labeling

(A) Schematic of the experimental design. In a parallel experiment as shown in Figure 1, 6-week-old mice were fasted for 3 h, gavaged with $^{13}C_6$-glucose, and euthanized by decapitation (top) or microwave fixation (bottom), and brain regions were then dissected, flash frozen, and analyzed by GCMS.

(B) Schematic showing the stable isotope tracing glucose in glycolysis and TCA cycle and subsequent interpretations.

(C) Representative isotopologue for M6 of glycogen, glucose, and G6P; M2 of citrate, fumarate, malate, glutamate, glutamine, GABA, aspartate, and serine; and M3 of DHAP, 3PG, PEP, pyruvate, lactate, citrate, fumarate, malate, glutamate, glutamine, GABA, aspartate, and serine within the cortex regions between mice subjected to enzyme inactivation at CP and FM. Values are presented as mean ± SEM (n = 3 biological replicates), *p < 0.05, **p < 0.01, ***p < 0.001, #p < 0.0001, analyzed by Student's t test.

(D) Model of changes in glucose utilization within cortex between enzyme inactivation at CP and FM. Bolded red arrows represent overutilized pathways during the 90 s enzyme inactivation.

G6P, glucose 6-phosphate; DHAP, dihydroxyacetone phosphate; 3PG, 3-phosphoglyceric acid; PEP, phosphoenolpyruvate.

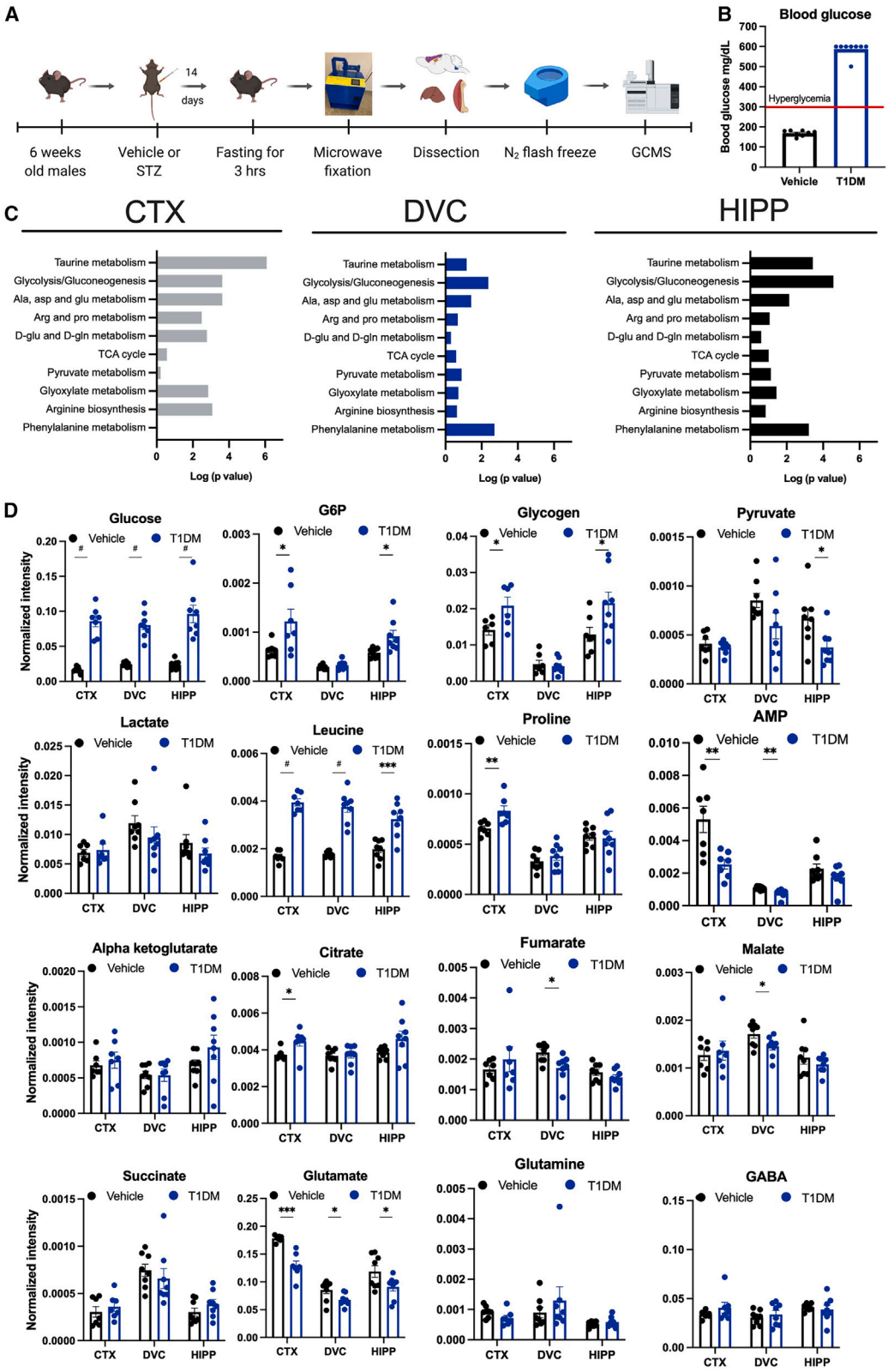

(legend on next page)

GLUT3 expression in the different brain regions (Figure S6); however, GLUT2, a neuronal glucose transporter, displays a 15%–70% decrease of positive areas across the CTX, HIPP, and DVC (Figure 5A). We observed a similar decrease in PDH and PC protein by IF in cortical regions and the DVC (Figures 5B and S6). Interestingly, the Cornu Ammonis 3 (CA3) neuronal layer of HIPP was the only subregion affected by hyperglycemia, while the CA1 and CA2 layers exhibited no differences in protein expression between PC and PDH assessed by IF (Figures 5B and S6).

DISCUSSION

There is a major scientific interest in deepening our understanding of the brain metabolome,[58,59] as many speculate it will aid in our understanding of brain physiology and could be key to understanding neurological disease pathology. In this study, we employed FM to create a snapshot of the brain metabolome through *in situ* heat inactivation and fixation of metabolic enzymes. We observed a number of interesting differences between FM (0.6 s) and CP (90 s), primarily increases in glycogen, glucose, citrate, and aKG but decreases in lactate, succinate, and malate in mouse brain fixed *in situ* with FM vs. CP. These data suggest increased utilization of glycogen and glucose for glycolysis and lactate production, as well as TCA cycle anaplerosis during the 90 s interval to preserve metabolites via CP. Interestingly, the metabolic shifts toward lactate production and anaplerosis are often observed during hypoxia[60] and occur frequently during cancer metabolism.[61] It is worth noting that we did not observe a difference in amino acid abundances between FM and CP. Collectively, these data are in agreement with previously published *in vivo* NMR analyses that support FM fixation to preserve physiological brain metabolome.[41–43]

Stable isotope tracing is a powerful technique to study metabolic flux and enzyme activity *in vivo* and is frequently used to study brain metabolism.[21,62] Using isotopic tracing, we observed evidence of increased glucose and glycogen utilization demonstrated by decreased M6 isotopologue enrichment of glucose and glycogen and increased M3 isotopologue enrichment of 3-PG during 90 s of CP. To our surprise, we did not observe major changes in isotopic enrichment of TCA cycle metabolites. M2 and M3 isotopologues of citrate, fumarate, and malate were consistent between FM and CP. These data imply that although the total pool of metabolites decreased during 90 s of CP, the tissues seem to utilize both pools of unlabeled and labeled metabolites equally. Based on these data, we recommend the use of stable isotope tracing to study brain metabolism when FM is not available.

T1DM affects about 20 million people worldwide and leads to vascular diseases, retinopathy, neuropathy, and liver disease.[63] Recent reports have highlighted the impact of T1DM on brain glucose metabolism, and patients with T1DM have increased risk of developing late-onset dementia.[64] In the STZ-treated mouse model of T1DM fixed by FM, we did not observe major changes in pooled metabolites except for glucose and glycogen, which remained higher in the vehicle cohort. We then performed ^{13}C-glucose tracing through oral gavage. We observed glucose hypometabolism in all three regions we examined. Decreased enrichment of glycolytic and TCA cycle isotopologues were noted in multiple regions of the brain including the CTX, HIPP, and DVC. These data are in agreement with previous reports showing brain glucose hypometabolism in patients with T1DM,[65–69] glycogenolysis,[67,70] and increased hepatic glucose production.[71–74] Notably, glucose metabolism differed between the CTX and the DVC within the T1DM cohort. It is worth noting that the blood-brain barrier is permeable throughout much of the DVC, and this region could have alternative metabolic controls compared with the CTX and HIPP.

Limitation of study

We would like to highlight that rodent brain metabolism is highly sensitive to stimuli such as handling and stress,[75] anesthesia,[76] and time post-euthanasia.[29] Future studies should focus on isolating single-cell types to define the cell type-specific brain metabolism in healthy and diseased tissue. It would also be of interest to test whether FM is compatible with new single-cell technologies such as matrix-assisted laser desorption ionization (MALDI) MS imaging,[17] single-cell RNA sequencing (RNA-seq),[77] and spatial proteomics analyses.[78,79]

STAR★METHODS

Detailed methods are provided in the online version of this paper and include the following:

- KEY RESOURCES TABLE
- RESOURCE AVAILABILITY
  - Lead contact
  - Materials availability
  - Data and code availability
- EXPERIMENTAL MODEL AND SUBJECT DETAILS
  - Animals
- METHOD DETAILS
  - Chemicals and reagents
  - Induction of hyperglycemia and *in vivo* glucose assessments
  - Gavage of [U-13C] glucose
  - Microwave fixation
  - Immunofluorescence
  - Sample preparation

Figure 3. Pooled metabolomics analysis of mouse brain from a model of T1DM using FM

(A) Schematic of the experimental design. 6-week-old mice were injected with either vehicle or 200 mg/kg STZ to induce hyperglycemia. After 14 days, mice were fasted for 3 h and euthanized by focused microwave (FM). Brain regions were then dissected, flash frozen, and analyzed by GCMS.

(B) Blood glucose levels measured by hand-held glucometer in vehicle and T1DM mice after 14 days of hyperglycemia (n = 8 biological replicates).

(C) Pathway analysis (performed by Metaboanalyst) of CTX, DVC, and HIPP between vehicle-treated and T1DM mice.

(D) Representative metabolite levels from glycogen metabolism, glycolysis, and TCA cycle between vehicle and T1DM.

Values are presented as mean ± SEM (n = 6–8 biological replicates), *p < 0.05, **p < 0.01, ***p < 0.001, #p < 0.0001, analyzed by Student's t test.

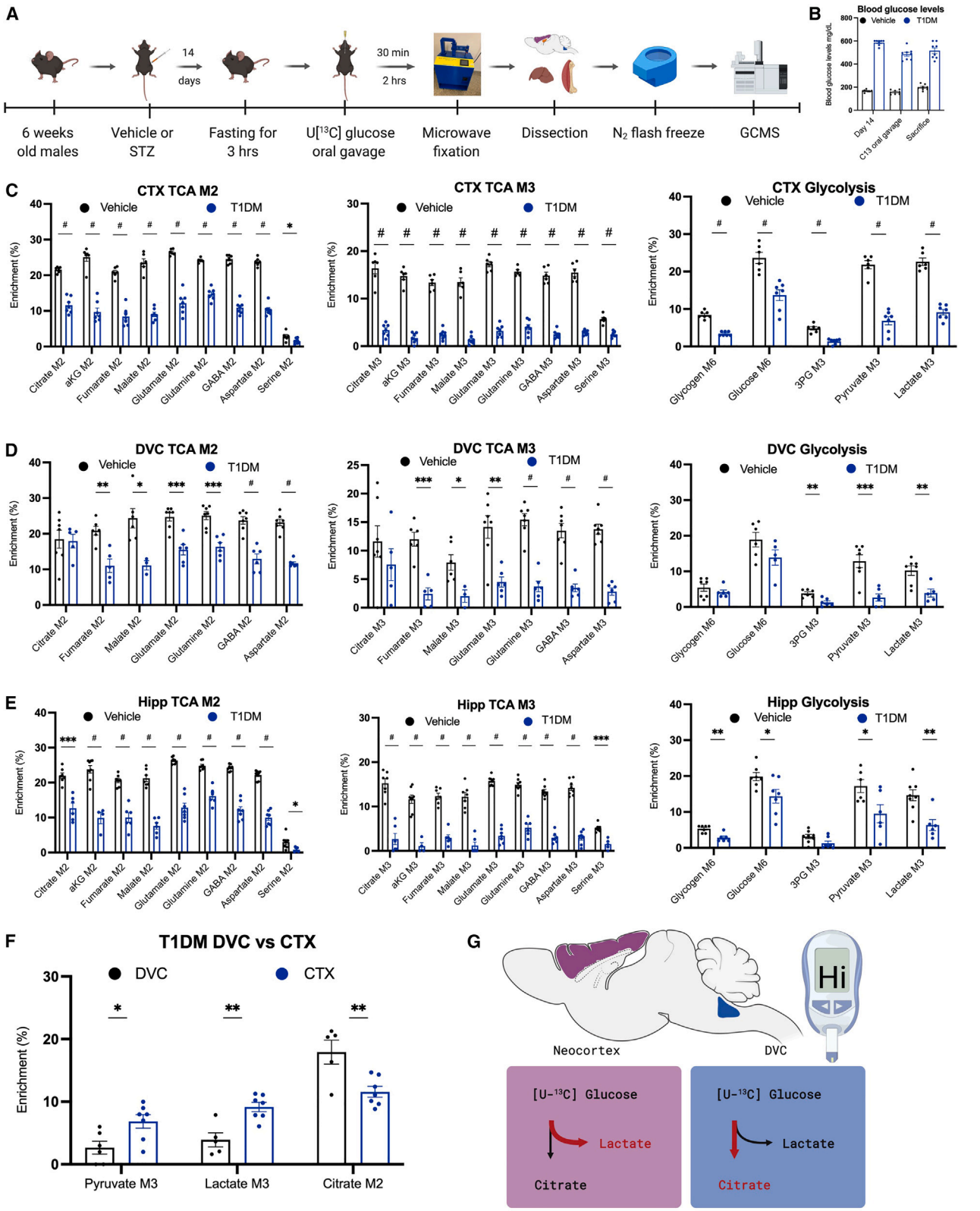

(legend on next page)

- Pellet hydrolysis
- Sample derivatization
- GCMS quantification

- QUANTIFICATION AND STATISTICAL ANALYSIS

SUPPLEMENTAL INFORMATION

Supplemental information can be found online at https://doi.org/10.1016/j.crmeth.2023.100455.

ACKNOWLEDGMENTS

This study was supported by National Institutes of Health (NIH) grants R35 NS116824 (M.S.G.), P01 NS097197 (M.S.G.), R01 AG066653 (R.C.S.), and R01 CA266004 (R.C.S.); NIH NIDDK R01 DK122811 (B.N.S.); NIH NINDS R01 NS092552 (B.N.S.); NIH/NCI F99CA264165 (L.E.A.Y.); NIH/NCI training grant T32CA165990 (L.R.C.); and a V-Scholar grant (R.C.S.).

AUTHOR CONTRIBUTIONS

Conceptualization, R.C.S., B.N.S., and J.A.J.; methodology, R.C.S., B.N.S., and J.A.J.; investigation, J.A.J., M.B.W., L.E.A.Y., K.H.M., T.R.H., M.D.B., K.E.B., P.T.C., M.I.W., L.P.Y.S., W.C.S., R.C.B., L.R.C., and C.W.; writing – original draft, R.C.S. and J.A.J.; writing – review & editing, R.C.S., J.A.J., L.E.A.Y., L.R.C., T.R.H., B.N.S., and M.S.G.; funding acquisition, R.C.S., M.S.G., and B.N.S.; resources, R.C.S., M.S.G., and B.N.S.; supervision, R.C.S., M.S.G., and B.N.S.

DECLARATION OF INTERESTS

R.C.S. has research support and received consultancy fees from Maze Therapeutics. R.C.S. is a cofounder of Attrogen, LLC. R.C.S. is a member of the Medical Advisory Board for Little Warrior Foundation. M.S.G. has research support and research compounds from Maze Therapeutics, Valerion Therapeutics, and Ionis Pharmaceuticals. M.S.G. also received consultancy fees from Maze Therapeutics, PTC Therapeutics, Aro Biotherapeutics, and the Glut1-Deficiency Syndrome Foundation. M.S.G. and R.C.B. are cofounders of Attrogen, LLC.

Received: October 19, 2022
Revised: February 14, 2023
Accepted: March 27, 2023
Published: April 18, 2023

REFERENCES

1. Erbsloh, F., Bernsmeier, A., and Hillesheim, H.R. (1958). The glucose consumption of the brain & its dependence on the liver. Archiv for. Psychiatrie und Zeitschrift f. d. ges. Neurologie *196*, 611–626. https://doi.org/10.1007/BF00344388.
2. Díaz-García, C.M., and Yellen, G. (2019). Neurons rely on glucose rather than astrocytic lactate during stimulation. J. Neurosci. Res. *97*, 883–889.
3. Dienel, G.A. (2019). Brain glucose metabolism: integration of energetics with function. Physiol. Rev. *99*, 949–1045.
4. Nimgampalle, M., Chakravarthy, H., and Devanathan, V. (2021). Glucose metabolism in the brain: an update. In Recent Developments in Applied Microbiology and Biochemistry (Elsevier), pp. 77–88.
5. Sibson, N.R., Mason, G.F., Shen, J., Cline, G.W., Herskovits, A.Z., Wall, J.E., Behar, K.L., Rothman, D.L., and Shulman, R.G. (2001). In vivo13C NMR measurement of neurotransmitter glutamate cycling, anaplerosis and TCA cycle flux in rat brain during [2-13C] glucose infusion. J. Neurochem. *76*, 975–989.
6. Sun, R.C., Fan, T.W.-M., Deng, P., Higashi, R.M., Lane, A.N., Le, A.-T., Scott, T.L., Sun, Q., Warmoes, M.O., and Yang, Y. (2017). Noninvasive liquid diet delivery of stable isotopes into mouse models for deep metabolic network tracing. Nat. Commun. *8*, 1646–1710.
7. Conroy, L.R., Hawkinson, T.R., Young, L.E.A., Gentry, M.S., and Sun, R.C. (2021). Emerging roles of N-linked glycosylation in brain physiology and disorders. Trends Endocrinol. Metabol. *32*, 980–993.
8. Telser, A., Robinson, H.C., and Dorfman, A. (1966). The biosynthesis of chondroitin sulfate. Arch. Biochem. Biophys. *116*, 458–465.
9. Sugahara, K., and Kitagawa, H. (2002). Heparin and heparan sulfate biosynthesis. IUBMB Life *54*, 163–175.
10. Mosconi, L., Tsui, W.H., Herholz, K., Pupi, A., Drzezga, A., Lucignani, G., Reiman, E.M., Holthoff, V., Kalbe, E., Sorbi, S., et al. (2008). Multicenter standardized 18F-FDG PET diagnosis of mild cognitive impairment, Alzheimer's disease, and other dementias. J. Nucl. Med. *49*, 390–398.
11. Walker, Z., Gandolfo, F., Orini, S., Garibotto, V., Agosta, F., Arbizu, J., Bouwman, F., Drzezga, A., Nestor, P., Boccardi, M., et al. (2018). Clinical utility of FDG PET in Parkinson's disease and atypical parkinsonism associated with dementia. Eur. J. Nucl. Med. Mol. Imag. *45*, 1534–1545.
12. Willmann, O., Wennberg, R., May, T., Woermann, F.G., and Pohlmann-Eden, B. (2007). The contribution of 18F-FDG PET in preoperative epilepsy surgery evaluation for patients with temporal lobe epilepsy: a meta-analysis. Seizure *16*, 509–520.
13. Pascual, J.M., Van Heertum, R.L., Wang, D., Engelstad, K., and De Vivo, D.C. (2002). Imaging the metabolic footprint of Glut1 deficiency on the brain. Ann. Neurol. *52*, 458–464.
14. Baranwal, A., Mirbolooki, M.R., and Mukherjee, J. (2015). Initial assessment of β3-adrenoceptor-activated Brown adipose tissue in streptozotocin-induced type 1 diabetes rodent model using [18F]fluorodeoxyglucose positron emission tomography/computed tomography. Mol. Imag. *14*, 22–33. https://doi.org/10.2310/7290.2015.00028.
15. Monsorno, K., Buckinx, A., and Paolicelli, R.C. (2022). Microglial metabolic flexibility: emerging roles for lactate. Trends in Endocrinology & Metabolism *33*, 186–195.
16. Zhao, Y., and Xu, H. (2022). Microglial lactate metabolism as a potential therapeutic target for Alzheimer's disease. Mol. Neurodegener. *17*, 36–43.

Figure 4. Stable isotope labeling in the brain of a mouse model of T1DM using FM

(A) Schematic of the experimental design. 6-week-old mice were injected with either vehicle or 200 mg/kg of streptozotocin (STZ) to induce hyperglycemia. After 14 days, mice were fasted for 3 h, gavaged with $^{13}C_6$-glucose, and euthanized by focused microwave (FM). Brain regions were then dissected, flash frozen, and analyzed by GCMS.

(B) Blood glucose levels were measured by hand-held glucometer before fasting, before tracer gavage delivery, and before microwave fixation (n = 8).

(C–E) Representative isotopologue enrichment for M6 of glycogen and glucose; M2 of citrate, aKG, fumarate, malate, glutamate, glutamine, GABA, aspartate, and serine; and M3 of 3PG, pyruvate, lactate, citrate, aKG, fumarate, malate, glutamate, glutamine, GABA, aspartate, and serine for three brain regions, CTX (C), DVC (D), and HIPP (E), of T1DM mice. Values are presented as mean ± SEM (n = 6–8 biological replicates).

(F) M3 isotopologues of pyruvate and lactate and M2 isotopologue of citrate between CTX and DVC in T1DM. Values are presented as mean ± SEM (n = 6–7 biological replicates).

(G) Model of changes in glucose utilization in CTX and DVC and in T1DM.

3PG, 3-phosphoglyceric acid; aKG, alpha-ketoglutarate.

*p < 0.05, **p < 0.01, ***p < 0.001, #p < 0.0001, analyzed by Student's t test.

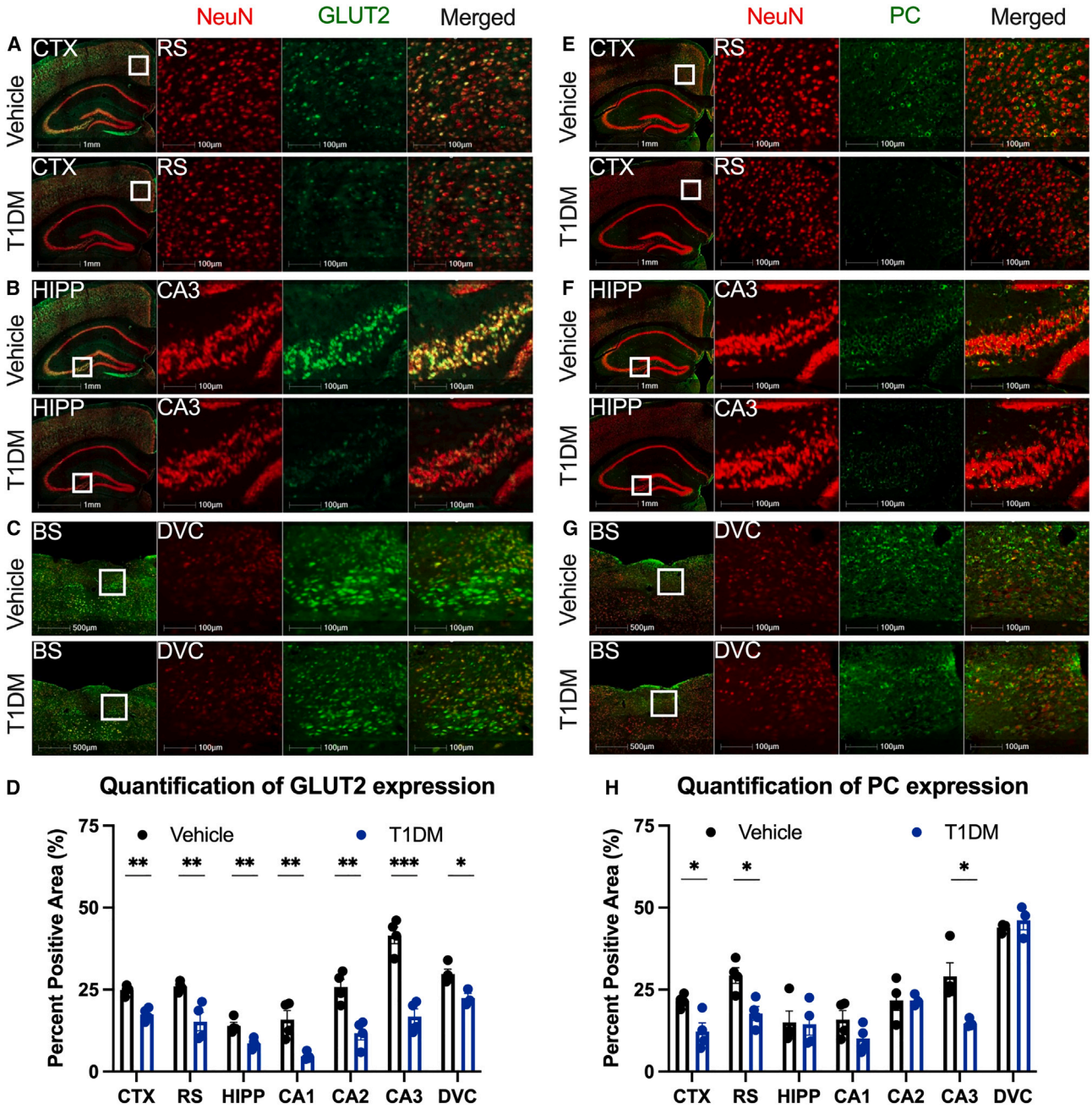

Figure 5. Immunofluorescent analysis of GLUT2 and PC expression in CTX, HIPP, and BS in a mouse model of T1DM

(A–C) 20 μm coronal sections of the mouse brain were stained with GLUT2 (green) and NeuN (red) and quantified in in the CTX (A), HIPP (B), and brainstem (BS) (C). Zoomed-in images are shown for the retro-splenial (RS) cortex, Cornu Ammonis 3 (CA3) of HIPP, and the DVC of BS.

(D) Quantification of % positive pixels for GLUT2 using HALO software.

(E–G) 20 μm coronal sections of the mouse brain were stained with pyruvate carboxylase (PC) (green) and NeuN (red) and quantified in in the CTX (E), HIPP (F), and BS (G). Zoomed-in images are shown for the RS, the CA3 of HIPP, and the DVC of BS.

(H) Quantification of percentage of positive pixels for PC using HALO software.

Values are presented as mean ± SEM (n = 4 biological replicates), *p < 0.05, **p < 0.01, ***p < 0.001, analyzed by Student's t test. Scale bars are either 1 mm, 500 μm, or 100 μm.

PC, pyruvate carboxylase; GLUT2, glucose transporter 2.

17. Hawkinson, T.R., Young, L.E.A., Conroy, L.R., Clarke, H.A., Gentry, M.S., and Sun, R.C. (2021). In situ spatial glycomic imaging of mouse and human alzheimerżs disease brains. Alzheimer's Dementia *18*, 1721–1735. https://doi.org/10.1002/alz.12523.

18. Jakkamsetti, V., Marin-Valencia, I., Ma, Q., Good, L.B., Terrill, T., Rajasekaran, K., Pichumani, K., Khemtong, C., Hooshyar, M.A., Sundarrajan, C., et al. (2019). Brain metabolism modulates neuronal excitability in a mouse model of pyruvate dehydrogenase deficiency. Sci. Transl. Med. *11*, eaan0457.

19. Muccioli, L., Farolfi, A., Pondrelli, F., d'Orsi, G., Michelucci, R., Freri, E., Canafoglia, L., Licchetta, L., Toni, F., Bonfiglioli, R., et al. (2020). FDG-PET assessment and metabolic patterns in Lafora disease. Eur. J. Nucl. Med. Mol. Imag. *47*, 1576–1584.

20. Hepowit, N.L., Macedo, J.K.A., Young, L.E.A., Liu, K., Sun, R.C., MacGurn, J.A., and Dickson, R.C. (2021). Enhancing lifespan of budding yeast by pharmacological lowering of amino acid pools. Aging (Albany NY) *13*, 7846–7871.

21. Maher, E.A., Marin-Valencia, I., Bachoo, R.M., Mashimo, T., Raisanen, J., Hatanpaa, K.J., Jindal, A., Jeffrey, F.M., Choi, C., Madden, C., et al. (2012). Metabolism of [U-13C] glucose in human brain tumors in vivo. NMR Biomed. *25*, 1234–1244.

22. Choi, C., Ganji, S.K., DeBerardinis, R.J., Hatanpaa, K.J., Rakheja, D., Kovacs, Z., Yang, X.-L., Mashimo, T., Raisanen, J.M., Marin-Valencia, I., et al. (2012). 2-hydroxyglutarate detection by magnetic resonance spectroscopy in IDH-mutated patients with gliomas. Nat. Med. *18*, 624–629.

23. Merritt, M.E., Harrison, C., Storey, C., Jeffrey, F.M., Sherry, A.D., and Malloy, C.R. (2007). Hyperpolarized 13C allows a direct measure of flux through a single enzyme-catalyzed step by NMR. Proc. Natl. Acad. Sci. USA *104*, 19773–19777.

24. Ghini, V., Unger, F.T., Tenori, L., Turano, P., Juhl, H., and David, K.A. (2015). Metabolomics profiling of pre-and post-anesthesia plasma samples of colorectal patients obtained via Ficoll separation. Metabolomics *11*, 1769–1778. https://doi.org/10.1007/s11306-015-0832-5.

25. Lei, H., Duarte, J.M.N., Mlynarik, V., Python, A., and Gruetter, R. (2010). Deep thiopental anesthesia alters steady-state glucose homeostasis but not the neurochemical profile of rat cortex. J. Neurosci. Res. *88*, 413–419. https://doi.org/10.1002/jnr.22212.

26. Brewer, M.K., Uittenbogaard, A., Austin, G.L., Segvich, D.M., DePaoli-Roach, A., Roach, P.J., McCarthy, J.J., Simmons, Z.R., Brandon, J.A., Zhou, Z., et al. (2019). Targeting pathogenic Lafora bodies in Lafora disease using an antibody-enzyme fusion. Cell Metabol. *30*, 689–705.e6.

27. Duran, J., Hervera, A., Markussen, K.H., Varea, O., López-Soldado, I., Sun, R.C., Del Río, J.A., Gentry, M.S., and Guinovart, J.J. (2021). Astrocytic glycogen accumulation drives the pathophysiology of neurodegeneration in Lafora disease. Brain *144*, 2349–2360.

28. Friede, R.L., and van Houten, W.H. (1961). Relations between post-mortem alterations and glycolytic metabolism in the brain. Exp. Neurol. *4*, 197–204.

29. Rauckhorst, A.J., Borcherding, N., Pape, D.J., Kraus, A.S., Scerbo, D.A., and Taylor, E.B. (2022). Mouse tissue harvest-induced hypoxia rapidly alters the in vivo metabolome, between-genotype metabolite level differences, and 13C-tracing enrichments. Preprint at bioRxiv. https://doi.org/10.1101/2022.06.07.495179.

30. Suarez, R.K., Staples, J.F., Lighton, J.R., and West, T.G. (1997). Relationships between enzymatic flux capacities and metabolic flux rates: nonequilibrium reactions in muscle glycolysis. Proc. Natl. Acad. Sci. USA *94*, 7065–7069.

31. Slavov, N., Budnik, B.A., Schwab, D., Airoldi, E.M., and van Oudenaarden, A. (2014). Constant growth rate can be supported by decreasing energy flux and increasing aerobic glycolysis. Cell Rep. *7*, 705–714.

32. Shestov, A.A., Liu, X., Ser, Z., Cluntun, A.A., Hung, Y.P., Huang, L., Kim, D., Le, A., Yellen, G., Albeck, J.G., and Locasale, J.W. (2014). Quantitative determinants of aerobic glycolysis identify flux through the enzyme GAPDH as a limiting step. Elife *3*, e03342.

33. French, T.J., Goode, A.W., and Sugden, M.C. (1986). Ischaemia and tissue pyruvate dehydrogenase activities in the rat: a comparison of the effects of cervical dislocation and pentobarbital anaesthesia. Biochem. Int. *13*, 843–852.

34. Zalewska, T., and Domanska-Janik, K. (1979). Energy utilization and changes in some intermediates of glucose metabolism in normal and hypoxic rat brain after decapitation. Resuscitation *7*, 199–205.

35. Overmyer, K.A., Thonusin, C., Qi, N.R., Burant, C.F., and Evans, C.R. (2015). Impact of anesthesia and euthanasia on metabolomics of mammalian tissues: studies in a C57BL/6J mouse model. PLoS One *10*, e0117232.

36. DiNuzzo, M., Walls, A.B., Öz, G., Seaquist, E.R., Waagepetersen, H.S., Bak, L.K., Nedergaard, M., and Schousboe, A. (2019). State-dependent changes in brain glycogen metabolism. Adv. Neurobiol. *23*, 269–309.

37. O'Callaghan, J.P., and Sriram, K. (2004). Focused microwave irradiation of the brain preserves in vivo protein phosphorylation: comparison with other methods of sacrifice and analysis of multiple phosphoproteins. J. Neurosci. Methods *135*, 159–168.

38. English, N.J., and MacElroy, J.M.D. (2003). Molecular dynamics simulations of microwave heating of water. J. Chem. Phys. *118*, 1589–1592.

39. Mayers, C.P. (1970). Histological fixation by microwave heating. J. Clin. Pathol. *23*, 273–275.

40. Login, G.R. (1978). Microwave fixation versus formalin fixation of surgical and autopsy tissue. Am. J. Med. Technol. *44*, 435–437.

41. De Graaf, R.A., Chowdhury, G.M.I., Brown, P.B., Rothman, D.L., and Behar, K.L. (2009). In situ 3D magnetic resonance metabolic imaging of microwave-irradiated rodent brain: a new tool for metabolomics research. J. Neurochem. *109*, 494–501.

42. Detour, J., Elbayed, K., Piotto, M., Moussallieh, F.M., Nehlig, A., and Namer, I.J. (2011). Ultra fast in vivo microwave irradiation for enhanced metabolic stability of brain biopsy samples during HRMAS NMR analysis. J. Neurosci. Methods *201*, 89–97.

43. Hsu, C.H., Lin, S., Ho, A.C., Johnson, T.D., Wang, P.C., Scafidi, J., and Tu, T.W. (2021). Comparison of in vivo and in situ detection of hippocampal metabolites in mouse brain using 1H-MRS. NMR Biomed. *34*, e4451.

44. Boychuk, C.R., and Smith, B.N. (2016). Glutamatergic drive facilitates synaptic inhibition of dorsal vagal motor neurons after experimentally induced diabetes in mice. J. Neurophysiol. *116*, 1498–1506. https://doi.org/10.1152/jn.00325.2016.

45. Halmos, K.C., Gyarmati, P., Xu, H., Maimaiti, S., Jancsó, G., Benedek, G., and Smith, B.N. (2015). Molecular and functional changes in glucokinase expression in the brainstem dorsal vagal complex in a murine model of type 1 diabetes. Neuroscience *306*, 115–122. https://doi.org/10.1016/j.neuroscience.2015.08.023.

46. Andres, D.A., Young, L.E.A., Veeranki, S., Hawkinson, T.R., Levitan, B.M., He, D., Wang, C., Satin, J., and Sun, R.C. (2020). Improved workflow for mass spectrometry–based metabolomics analysis of the heart. J. Biol. Chem. *295*, 2676–2686.

47. Williams, H.C., Piron, M.A., Nation, G.K., Walsh, A.E., Young, L.E.A., Sun, R.C., and Johnson, L.A. (2020). Oral gavage delivery of stable isotope tracer for in vivo metabolomics. Metabolites *10*, 501.

48. Young, L.E.A., Brizzee, C.O., Macedo, J.K.A., Murphy, R.D., Contreras, C.J., DePaoli-Roach, A.A., Roach, P.J., Gentry, M.S., and Sun, R.C. (2020). Accurate and sensitive quantitation of glucose and glucose phosphates derived from storage carbohydrates by mass spectrometry. Carbohydr. Polym. *230*, 115651. https://doi.org/10.1016/j.carbpol.2019.115651.

49. Pitra, S., and Smith, B.N. (2021). Musings on the wanderer: what's new in our understanding of vago-vagal reflexes? VI. Central vagal circuits that control glucose metabolism. Am. J. Physiol. Gastrointest. Liver Physiol. *320*, G175-g182. https://doi.org/10.1152/ajpgi.00368.2020.

50. Kaushik, A.K., and DeBerardinis, R.J. (2018). Applications of metabolomics to study cancer metabolism. Biochim. Biophys. Acta Rev. Canc *1870*, 2–14.

51. Johnston, K., Pachnis, P., Tasdogan, A., Faubert, B., Zacharias, L.G., Vu, H.S., Rodgers-Augustyniak, L., Johnson, A., Huang, F., Ricciardo, S., et al. (2021). Isotope tracing reveals glycolysis and oxidative metabolism in childhood tumors of multiple histologies. Med *2*, 395–410.

52. Jolivalt, C.G., Calcutt, N.A., and Masliah, E. (2012). Similar pattern of peripheral neuropathy in mouse models of type 1 diabetes and Alzheimer's disease. Neuroscience *202*, 405–412.

53. Li, W., Huang, E., and Gao, S. (2017). Type 1 diabetes mellitus and cognitive impairments: a systematic review. J. Alzheimers Dis. *57*, 29–36.

54. Bolla, A.M., Butera, E., Pellegrini, S., Caretto, A., Bonfanti, R., Zuppardo, R.A., Barera, G., Cavestro, G.M., Sordi, V., and Bosi, E. (2020). Expression of glucose transporters in duodenal mucosa of patients with type 1 diabetes. Acta Diabetol. *57*, 1367–1373. https://doi.org/10.1007/s00592-020-01558-w.

55. Wasik, A.A., and Lehtonen, S. (2018). Glucose transporters in diabetic kidney disease-friends or foes? Front. Endocrinol. *9*, 155. https://doi.org/10.3389/fendo.2018.00155.

56. Jiang, Y.K., Xin, K.Y., Ge, H.W., Kong, F.J., and Zhao, G. (2019). Upregulation of renal GLUT2 and SGLT2 is involved in high-fat diet-induced gestational diabetes in mice. Diabetes Metab. Syndr. Obes. *12*, 2095–2105. https://doi.org/10.2147/DMSO.S221396.

57. Szablewski, L. (2017). Glucose transporters in healthy heart and in cardiac disease. Int. J. Cardiol. *230*, 70–75. https://doi.org/10.1016/j.ijcard.2016.12.083.

58. de la Monte, S.M., and Tong, M. (2014). Brain metabolic dysfunction at the core of Alzheimer's disease. Biochem. Pharmacol. *88*, 548–559.

59. Cunnane, S., Nugent, S., Roy, M., Courchesne-Loyer, A., Croteau, E., Tremblay, S., Castellano, A., Pifferi, F., Bocti, C., Paquet, N., et al. (2011). Brain fuel metabolism, aging, and Alzheimer's disease. Nutrition *27*, 3–20.

60. Lee, D.C., Sohn, H.A., Park, Z.-Y., Oh, S., Kang, Y.K., Lee, K.-m., Kang, M., Jang, Y.J., Yang, S.-J., Hong, Y.K., et al. (2015). A lactate-induced response to hypoxia. Cell *161*, 595–609.

61. Ganapathy-Kanniappan, S., and Geschwind, J.-F.H. (2013). Tumor glycolysis as a target for cancer therapy: progress and prospects. Mol. Cancer *12*, 152–211.

62. McNair, L.F., Kornfelt, R., Walls, A.B., Andersen, J.V., Aldana, B.I., Nissen, J.D., Schousboe, A., and Waagepetersen, H.S. (2017). Metabolic characterization of acutely isolated hippocampal and cerebral cortical slices using [U-13C] glucose and [1, 2-13C] acetate as substrates. Neurochem. Res. *42*, 810–826.

63. Cade, W.T. (2008). Diabetes-related microvascular and macrovascular diseases in the physical therapy setting. Phys. Ther. *88*, 1322–1335. https://doi.org/10.2522/ptj.20080008.

64. Lacy, M.E., Gilsanz, P., Karter, A.J., Quesenberry, C.P., Pletcher, M.J., and Whitmer, R.A. (2018). Long-term glycemic control and dementia risk in type 1 diabetes. Diabetes Care *41*, 2339–2345. https://doi.org/10.2337/dc18-0073.

65. van Golen, L.W., Huisman, M.C., Ijzerman, R.G., Hoetjes, N.J., Schwarte, L.A., Lammertsma, A.A., and Diamant, M. (2013). Cerebral blood flow and glucose metabolism measured with positron emission tomography are decreased in human type 1 diabetes. Diabetes *62*, 2898–2904.

66. Basu, A., Basu, R., Shah, P., Vella, A., Johnson, C.M., Nair, K.S., Jensen, M.D., Schwenk, W.F., and Rizza, R.A. (2000). Effects of type 2 diabetes on the ability of insulin and glucose to regulate splanchnic and muscle glucose metabolism: evidence for a defect in hepatic glucokinase activity. Diabetes *49*, 272–283. https://doi.org/10.2337/diabetes.49.2.272.

67. Bischof, M.G., Krssak, M., Krebs, M., Bernroider, E., Stingl, H., Waldhäusl, W., and Roden, M. (2001). Effects of short-term improvement of insulin treatment and glycemia on hepatic glycogen metabolism in type 1 diabetes. Diabetes *50*, 392–398. https://doi.org/10.2337/diabetes.50.2.392.

68. Hwang, J.J., Jiang, L., Sanchez Rangel, E., Fan, X., Ding, Y., Lam, W., Leventhal, J., Dai, F., Rothman, D.L., Mason, G.F., and Sherwin, R.S. (2019). Glycemic variability and brain glucose levels in type 1 diabetes. Diabetes *68*, 163–171. https://doi.org/10.2337/db18-0722.

69. Krssak, M., Brehm, A., Bernroider, E., Anderwald, C., Nowotny, P., Dalla Man, C., Cobelli, C., Cline, G.W., Shulman, G.I., Waldhäusl, W., and Roden, M. (2004). Alterations in postprandial hepatic glycogen metabolism in type 2 diabetes. Diabetes *53*, 3048–3056. https://doi.org/10.2337/diabetes.53.12.3048.

70. Kishore, P., Gabriely, I., Cui, M.H., Di Vito, J., Gajavelli, S., Hwang, J.H., and Shamoon, H. (2006). Role of hepatic glycogen breakdown in defective counterregulation of hypoglycemia in intensively treated type 1 diabetes. Diabetes *55*, 659–666. https://doi.org/10.2337/diabetes.55.03.06.db05-0849.

71. Girard, J. (2017). Glucagon, a key factor in the pathophysiology of type 2 diabetes. Biochimie *143*, 33–36. https://doi.org/10.1016/j.biochi.2017.10.004.

72. Hatting, M., Tavares, C.D.J., Sharabi, K., Rines, A.K., and Puigserver, P. (2018). Insulin regulation of gluconeogenesis. Ann. N. Y. Acad. Sci. *1411*, 21–35. https://doi.org/10.1111/nyas.13435.

73. Lee, Y., Wang, M.Y., Du, X.Q., Charron, M.J., and Unger, R.H. (2011). Glucagon receptor knockout prevents insulin-deficient type 1 diabetes in mice. Diabetes *60*, 391–397. https://doi.org/10.2337/db10-0426.

74. Petersen, K.F., Price, T.B., and Bergeron, R. (2004). Regulation of net hepatic glycogenolysis and gluconeogenesis during exercise: impact of type 1 diabetes. J. Clin. Endocrinol. Metab. *89*, 4656–4664. https://doi.org/10.1210/jc.2004-0408.

75. Lee, K.W., Kim, J.B., Seo, J.S., Kim, T.K., Im, J.Y., Baek, I.S., Kim, K.S., Lee, J.K., and Han, P.L. (2009). Behavioral stress accelerates plaque pathogenesis in the brain of Tg2576 mice via generation of metabolic oxidative stress. J. Neurochem. *108*, 165–175.

76. Bonhomme, V., Boveroux, P., Hans, P., Brichant, J.F., Vanhaudenhuyse, A., Boly, M., and Laureys, S. (2011). Influence of anesthesia on cerebral blood flow, cerebral metabolic rate, and brain functional connectivity. Curr. Opin. Anaesthesiol. *24*, 474–479.

77. Li, S.-Q., Yu, Y., Han, J.-Z., Wang, D., Liu, J., Qian, F., Fan, G.-H., Bucala, R., and Ye, R.D. (2015). Deficiency of macrophage migration inhibitory factor attenuates tau hyperphosphorylation in mouse models of Alzheimer's disease. J. Neuroinflammation *12*, 177–211.

78. Ximerakis, M., Lipnick, S.L., Innes, B.T., Simmons, S.K., Adiconis, X., Dionne, D., Mayweather, B.A., Nguyen, L., Niziolek, Z., Ozek, C., et al. (2019). Single-cell transcriptomic profiling of the aging mouse brain. Nat. Neurosci. *22*, 1696–1708.

79. Jiang, S., Chan, C.N., Rovira-Clavé, X., Chen, H., Bai, Y., Zhu, B., McCaffrey, E., Greenwald, N.F., Liu, C., Barlow, G.L., et al. (2022). Combined protein and nucleic acid imaging reveals virus-dependent B cell and macrophage immunosuppression of tissue microenvironments. Immunity *55*, 1118–1134.e8.

80. Heinrich, P., Kohler, C., Ellmann, L., Kuerner, P., Spang, R., Oefner, P.J., and Dettmer, K. (2018). Correcting for natural isotope abundance and tracer impurity in MS-, MS/MS- and high-resolution-multiple-tracer-data from stable isotope labeling experiments with IsoCorrectoR. Sci Rep *8*, 17910. https://doi.org/10.1038/s41598-018-36293-4.

81. Dagley, M.J., and McConville, M.J. (2018). DexSI: a new tool for the rapid quantitation of ^{13}C-labelled metabolites detected by GC-MS. Bioinformatics *34*, 1957–1958. https://doi.org/10.1093/bioinformatics/bty025.

82. Xia, J., Psychogios, N., Young, N., and Wishart, D.S. (2009). MetaboAnalyst: a web server for metabolomic data analysis and interpretation. Nucleic Acids Research *7*, W652–W660. https://doi.org/10.1093/nar/gkp356.

83. Fiehn, O. (2016). Metablomics by gas chromatography—mass spectrometry: combined targeted and untargeted profiling. Curr. Protoc. Mol. Biol. *114*, 21.33.1–21.33.11. https://doi.org/10.1002/0471142727.mb3004s.

84. Fiehn, O., Kopka, J., Dörmann, P., Altmann, T., Trethewey, R.N., and Willmitzer, L. (2000). Metabolite profiling for plant functional genomics. Nat Biotechnol *18*, 1157–1161. https://doi.org/10.1038/81137.

85. Kind, T., Wohlgemuth, G., Lee, D.Y., Lu, Y., Palaoglu, M., Shahbaz, S., and Fiehn, O. (2009). FiehnLib: Mass Spectral and Retention Index Libraries for Metabolomics Based on Quadrupole and Time-of-Flight Gas Chromatography/Mass Spectrometry. Anal. Chem. *81*, 10038–10048. https://doi.org/10.1021/ac9019522.

STAR★METHODS

KEY RESOURCES TABLE

REAGENT or RESOURCE	SOURCE	IDENTIFIER
Antibodies		
GLUT1, Rabbit	Abcam	Cat# ab115730; RRID: AB_10903230
GLUT2, Rabbit	Novus	Cat# NBP2-22218; RRID: AB_2335858
GLUT3, Rabbit	Alomone	Cat# AGT-023; RRID:AB_2756644
Pyruvate Carboxylase, Rabbit	GeneTex	GTX121987
Pyruvate Dehydrogenase (ser 293), Rabbit	EMD Milipore	Cat# AP1062; RRID:AB_2863934
NeuN, Mouse	Abcam	ab279295
NeuN, Rabbit	Abcam	Cat# ab236870; RRID:AB_2927651
GFAP, Chicken	GeneTex	Cat# GTX85454; RRID:AB_10621124
DAPI	Novus	NBP2-31156
Goat anti-chicken, Alexa 594	Thermo Fisher Scientific	Cat# A-11042; RRID:AB_2534099
Goat anti-rabbit, Alexa 488	Thermo Fisher Scientific	Cat# A-11034; RRID:AB_2576217
Goat anti-mouse, Alexa 647	Thermo Fisher Scientific	Cat# A-21236; RRID:AB_2535805
Chemicals, peptides, and recombinant proteins		
U-13C6-glucose, 99%	Cambridge Isotope Laboratories	CLM-1396-MPT-PK
L-Norvaline	Sigma-Aldrich	N7627-5G
Methoxyamine hydrochloride	Sigma-Aldrich	226904-25G
Pyridine	Thermo Fisher Scientific	TS-27530
MSTFA +1 Percent TMCS	Sigma-Aldrich	375934-10X1ML
Hydrochloric Acid	Thermo Fisher Scientific	
HPLC Methanol	Thermo Fisher Scientific	34860-4X4L-R
PBS	Sigma-Aldrich	P3813
Heparin Sodium (10,000units/mL)	N/A	NDC# 25021040010
4% Paraformaldehyde in PBS	Thermo Fisher Scientific	J19943.K2
Sucrose	Thermo Fisher Scientific	036508.A1
Normal Goat Serum	Thermo Fisher Scientific	31873
Triton X-	Sigma-Aldrich	X100
Tween 20	Sigma-Aldrich	P1379
Prolong Glass	Thermo Fisher Scientific	P36984
Streptozotocin	Sigma-Aldrich	572201
Citric Acid	Thermo Fisher Scientific	A940
Sodium citrate dihydrate	Thermo Fisher Scientific	BP327
2-methylbutane	Thermo Fisher Scientific	019387AP
Ethanol	Decon Labs	CAS#: 64-17-5
OCT compound	Thermo Fisher Scientific	23-730-571
Deposited data		
Raw and processed metabolomics data	This study	Metabolomics Workbench ST002524 and ST002525
Software and algorithms		
HALO Software	Indica Labs	N/A
Prism	Graphpad	N/A
IsoCorrectoR	Heinrich et al.[80]	N/A
DEXSI software	Dagley and McConville[81]	N/A
Metaboanalyst	Xia et al.[82]	(https://chemdata.nist.gov/dokuwiki/doku.php?id=chemdata:amdis)

(*Continued on next page*)

Continued

REAGENT or RESOURCE	SOURCE	IDENTIFIER
AMDIS	Fiehn[83]; Fiehn et al.[84]; Kind et al[85]	(https://chemdata.nist.gov/dokuwiki/doku.php?id=chemdata:amdis)
Other		
Nova Max glucose test strips	ADW	#8548043523
Nova Max plus glucometer	ADW	#8548043435
High power-focused microwave	Muromachi Kikai Company	MMW-05
Animal Holder, TAW-174P	Muromachi Kikai Company	WJM-24 for 15-20g Mouse, WJM-28 for 20-40g Mouse, WJM-30 for 40-50g Mouse
60 mL syringe only, luer lock tip	BD Sciences	BD 309653
Over the head ear muffs	Fisher Scientific	19-130-1978
Safety Glasses	Fisher Scientific	19-181-514
N95 mask	Fisher Scientific	18-999-473

RESOURCE AVAILABILITY

Lead contact

Further information and requests for resources and reagents should be direct to and will be fulfilled by the lead contact, Ramon C. Sun (ramonsun@ufl.edu).

Materials availability

This study did not generate new unique reagents.

Data and code availability

- The raw and processed metabolomics datasets from this paper have been deposited at Metabolomics Workbench with accession number(s): ST002524 and ST002525.
- This paper does not report original code.
- Any additional information required to reanalyze the data reported in this paper is available from the lead contact upon request.

EXPERIMENTAL MODEL AND SUBJECT DETAILS

Animals

All experiments were performed on male C57BL6 background (000664; The Jackson Laboratory, Bar Harbor, ME), at 6 weeks of age. All mice used in the experiment were housed and cared for in the University of Kentucky Division of Laboratory Animal Resources facilities under normal 14:10 light-dark condition with food (Tekad Global pellets 2018, Indianapolis, IN) and water available *ad libitum*, except where noted. Experiments were carried out in accordance with the recommendations in the Guide for the Care and Use of Laboratory Animals of the University of Kentucky under protocols approved by the Institutional Animal Care and Use Committee (Protocol number:2020–3601). In total, 52 mice were used (n = 6 for untargeted metabolomics fixation study, n = 6 for ^{13}C glucose study, n = 16 for untargeted metabolomics study, n = 16 for ^{13}C glucose tracer study, n = 8 for IF). Randomization was done utilizing Excel and function RANDBETWEEN for each experiment, where 1 was control, and 2 was treatment. Cages were handled by altering descending cage card numbers one day and ascending the other day. Mice tissue was coded by 3 numbers and color code (for example 123 Black) to blind the samples during tissue harvest, and GCMS/IF prep. Data was unblinded to run statistics. If mice lost more than 20% of their original weight or were not exhibiting normal social or grooming behavior as per approved protocols, animals were euthanized.

METHOD DETAILS

Chemicals and reagents

HPLC grade methanol (34860-4X4L-R) and methoxyamine hydrochloride (226904-25G) were purchased from Sigma Aldrich (Burlington, MA, USA). Silylation Reagents, MSTFA +1% TMCS Reagent (TS-48915) and pyridine (TS-27530) were purchased from Thermo Fisher Scientific (Waltham, MA, USA). Amber vials (5184-3554), blue screw caps (5182-0717) were purchased from Agilent Technologies (Santa Clara, CA, USA). Streptozotocin (572201), PBS (P3813), Triton X-100 (X100), Tween 20 (P1379) were purchased from Sigma-Aldrich (St. Louis MO). Sodium citrate dihydrate (BP327), Citric acid anhydrous (A940) normal goat serum

(31873) and OCT compound (23-730-571), 2-methylbutane (019387AP), and ProlongGlass (P36984) from Thermo Fisher Scientific. [U-^{13}C] Glucose was obtained from Cambridge Isotope Laboratories (Tewksbury, MA, USA).

Induction of hyperglycemia and *in vivo* glucose assessments

At 6 weeks of age, mice were injected with streptozotocin (STZ; 200 mg/kg; i.p.; Sigma-Aldrich, St. Louis, MO) in citric acid (CA, 0.1M), after a 6 h fast. Mice were monitored daily for weight and blood glucose levels. Blood glucose levels were measured by handheld glucometer (Nova Max Plus; received from American Diabetes Wholesale (ADW), Pompano Beach, FL), using 0.3μL of blood from the tail vein. Nova Max glucose test strips were used (#8548043523, ADW). Blood concentration above 300 mg/dL was considered hyperglycemic. Mice were used for experiments after at least 14 days (14–16 days) of hyperglycemia.

Gavage of [U-13C] glucose

[U-^{13}C] Glucose (Cambridge Isotope Laboratories, Tewksbury, MA, USA) was dissolved in ddH_2O (Millipore Milli-Q, Bedford, MA, USA) based on the average mouse cohort bodyweight (2 g [U-^{13}C] glucose/kg bodyweight). After 3 h fast, 250 μL of glucose solution was administered via oral gavage. Tissues were collected at 30 min and 2 h. To assess the blood glucose levels before fasting, at tracer delivery and before microwave fixation handheld glucometer (Nova Max Plus; received from American Diabetes Wholesale, Pompano Beach, FL) was used.

Microwave fixation

Mice were euthanized by microwave fixation system at 5kW for 0.6 s (MMW-05, Muromachi Kikai Company, Japan). Brain regions (HIPP, CTX, DVC), as well as muscle and liver, were dissected post-mortem.

Immunofluorescence

Mice were transcardially perfused with Heparin-PBS (10 units/mL), followed by 4% PFA. Tissue was post-fixed for 24 h in 4% PFA and then cryoprotected with 30% sucrose in 0.01M PBS. The tissue was frozen with isopentanes and cut at 20μm with a sliding microtome. Staining was done free-floating in 24-well plates without inserts. Tissue was rinsed with 0.01M PBS, incubated for 1 h in 5% normal goat serum in 0.3% Triton X-100 in PBS. The tissue was then incubated at room temperature in the primary antibody (see STAR Methods) at diluted in 1% normal goat serum, followed by 3 × 15 min rinses in 0.05% Tween 20 in PBS. Tissue was then incubated for 1 h in secondary antibody diluted in 1% normal goat serum in PBS. For multiple labeling, primary antibodies were incubated for 2 h, and secondary antibodies for 1 h. Tissue was then exposed to DAPI for 5 min, mounted on the slides and cover slipped with Prolong Glass. Digital images were acquired through the Zeiss Axio Scan Z.7 digital slide scanner at 20× magnification and 12 Z-stacks. Figures were captured using HALO software (v3.3.2541.345, Indica Labs, Albuquerque, NM). Analysis was done by outlining the regions of interest in the HALO software and quantifying the positive pixels.

Primary antibodies	Host	Company and catalog #	Dilution	Conditions
GLUT1	Rabbit	Abcam ab115730	1:200	Overnight, RT
GLUT2	Rabbit	Novus NBP2-22218	1:200	Overnight, RT
GLUT3	Rabbit	Alomone AGT-023	1:200	Overnight, RT
Pyruvate Carboxylase	Rabbit	GeneTex GTX121987	1:200	Overnight, RT
Pyruvate Dehydrogenase (ser 293)	Rabbit	EMD Millipore AP1062	1:200	Overnight, RT
NeuN	Mouse	Abcam ab279295	1:1000	1 h, RT
NeuN	Rabbit	Abcam ab236870	1:1000	1 h, RT
GFAP	Chicken	GeneTex GTX85454	1:2000	2 h, RT
DAPI		Novus NBP2-31156	1:5000	5 min, RT

Secondary antibodies	Fluorophore	Company and catalog #	Dilution	Conditions
Goat anti-chicken	Alexa 594	A-11042	1:400	1 h, RT
Goat anti-rabbit	Alexa 488	A-11034	1:400	1 h, RT
Goat anti-mouse	Alexa 647	A-21236	1:400	1 h, RT

Sample preparation

Brains were removed immediately postmortem, and washed once with PBS, twice with diH_2O, blotted dry, and snap frozen in liquid nitrogen. Other set of brains were snap frozen after microwave fixation as described above. The frozen tissues were pulverized to 10 μm particles in liquid N_2 using a Freezer/Mill Cryogenic Grinder (SPEX SamplePrep). Brain regions were extracted with 1mL of 50% methanol in the grinder, while for muscle and liver twenty milligrams of each pulverized tissue were extracted in 1mL of 50% methanol and separated into polar (aqueous layer), and protein/DNA/RNA/glycogen pellet. The polar fraction was dried at 10^{-3} mBar using a SpeedVac (Thermo) followed by derivatization.

Pellet hydrolysis

Hydrolysis of the protein/DNA/RNA/glycogen pellet was performed by first resuspending the dried pellet in diH_2O followed by the addition of equal parts 2N HCl. Samples were vortexed thoroughly and incubated at 95°C for 2 h. The reaction was quenched with 100% methanol with 40μM L-norvaline (as an internal control). The sample was incubated on ice for 30 min and the supernatant was collected by centrifugation at 15,000 rpm at 4°C for 10 min. The collected supernatant was subsequently dried for 30 min by vacuum centrifuge at 10^{-3} mBar.

Sample derivatization

Dried polar and glycogen samples were derivatized by the addition of 20 mg/ml methoxyamine hydrochloride in pyridine and sequential addition of N-methyl-trimethylsilyl-trifluoroacetamide (MSTFA). Both reactions were incubated for 60 min at 60°C with thorough mixing in between addition of solvents. The mixture was then transferred to a v-shaped amber glass chromatography vial and analyzed by GCMS.

GCMS quantification

GCMS protocols were similar to those described previously with a modified temperature gradient was used for GC: Initial temperature was 130°C, held for 4 min, rising at 6 °C/min to 243°C, rising at 60 °C/min to 280°C, held for 2 min. The electron ionization (EI) energy was set to 70 eV. Scan (*m/z*:50–800) and full scan mode were used for metabolomics analysis. Mass spectra were translated to relative metabolite abundance using the Automated Mass Spectral Deconvolution and Identification System (AMDIS) software matched to the FiehnLib metabolomics library (available through Agilent) for retention time and fragmentation pattern matching with a confidence score of >80 (Fiehn, 2016; Fiehn et al., 2000; Kind et al., 2009). Data was further analyzed using the Data Extraction for Stable Isotope-labelled Metabolites (DEXSI) software package. Untargeted metabolomics data was normalized to total ion chromatogram. For glucose tracer raw data was exported and correction for natural abundance was done by IsoCorrectoR. Fractional enrichment of each metabolite was calculated as the relative abundance of each isotopologue relative to the sum of all other isotopologues. Mean enrichment was calculated as sum of fractional enrichment of labeled isotopologues (M1, M2, M3 …). For principal component analysis, pathway impact analysis the online tool Metaboanlyst was used (https://www.metaboanalyst.ca/). Data was auto scaled and log transformed.

QUANTIFICATION AND STATISTICAL ANALYSIS

Statistical analyses were carried out using GraphPad Prism. All numerical data are presented as mean ± SEM. Column analysis was performed using t-test. A p-value less than 0.05 was considered statistically significant. Statistical power and sample size calculations for animal studies were performed based on the current focused microwave dataset (CTX). A sample of n = 5/group would provide 80% power to detect a 3.1 standard deviation difference in the mean abundance level of a metabolomic feature between experimental groups based on a two-sample t-test at 5% significance level.